

Award Number: DAMD17-03-1-0541

TITLE: Automated Area Beam Equalization Mammography for Improved Imaging of Dense Breasts

PRINCIPAL INVESTIGATOR: Sabee Molloy, Ph.D.

CONTRACTING ORGANIZATION: University of California
Irvine, CA 92697

REPORT DATE: August 2005

TYPE OF REPORT: Final

PREPARED FOR: U.S. Army Medical Research and Materiel Command
Fort Detrick, Maryland 21702-5012

DISTRIBUTION STATEMENT: Approved for Public Release;
Distribution Unlimited

The views, opinions and/or findings contained in this report are those of the author(s) and should not be construed as an official Department of the Army position, policy or decision unless so designated by other documentation.

REPORT DOCUMENTATION PAGE

Form Approved
OMB No. 0704-0188

Public reporting burden for this collection of information is estimated to average 1 hour per response, including the time for reviewing instructions, searching existing data sources, gathering and maintaining the data needed, and completing and reviewing this collection of information. Send comments regarding this burden estimate or any other aspect of this collection of information, including suggestions for reducing this burden to Department of Defense, Washington Headquarters Services, Directorate for Information Operations and Reports (0704-0188), 1215 Jefferson Davis Highway, Suite 1204, Arlington, VA 22202-4302. Respondents should be aware that notwithstanding any other provision of law, no person shall be subject to any penalty for failing to comply with a collection of information if it does not display a currently valid OMB control number. PLEASE DO NOT RETURN YOUR FORM TO THE ABOVE ADDRESS.

1. REPORT DATE 01-08-2005		2. REPORT TYPE Final		3. DATES COVERED 15 Jul 2003 – 14 Jul 2005	
4. TITLE AND SUBTITLE Automated Area Beam Equalization Mammography for Improved Imaging of Dense Breasts				5a. CONTRACT NUMBER	
				5b. GRANT NUMBER DAMD17-03-1-0541	
				5c. PROGRAM ELEMENT NUMBER	
6. AUTHOR(S) Sabee Molloi, Ph.D.				5d. PROJECT NUMBER	
				5e. TASK NUMBER	
				5f. WORK UNIT NUMBER	
7. PERFORMING ORGANIZATION NAME(S) AND ADDRESS(ES) University of California Irvine, CA 92697				8. PERFORMING ORGANIZATION REPORT NUMBER	
9. SPONSORING / MONITORING AGENCY NAME(S) AND ADDRESS(ES) U.S. Army Medical Research and Materiel Command Fort Detrick, Maryland 21702-5012				10. SPONSOR/MONITOR'S ACRONYM(S)	
				11. SPONSOR/MONITOR'S REPORT NUMBER(S)	
12. DISTRIBUTION / AVAILABILITY STATEMENT Approved for Public Release; Distribution Unlimited					
13. SUPPLEMENTARY NOTES					
14. ABSTRACT In mammography, thick or dense breast regions persistently suffer from reduced contrast-to-noise ratio (CNR) because of degraded contrast from large scatter intensities and relatively high noise. Area x-ray beam equalization can improve image quality by increasing the x-ray exposure to underpenetrated regions without increasing the exposure to other breast regions. Optimal equalization parameters with respect to image quality and patient dose were determined through computer simulations and validated with experimental observations on a step phantom and an anthropomorphic breast phantom. Three parameters important in equalization digital mammography were considered: attenuator material ($Z = 13-92$), beam energy (22–34 kVp) and equalization level. A Mo/Mo digital mammography system was used for image acquisition. A prototype 16×16 piston driven equalization system was used for preparing patient-specific equalization masks. Simulation studies showed that a molybdenum attenuator and an equalization level of 20 were optimal for improving contrast, CNR and figure of merit (FOM = $CNR_2/dose$). Experimental measurements using these parameters showed significant improvements in contrast, CNR and FOM. Moreover, equalized images of a breast phantom showed improved image quality. These results indicate that area beam equalization can improve image quality in digital mammography.					
15. SUBJECT TERMS Breast imaging, Mammography					
16. SECURITY CLASSIFICATION OF:			17. LIMITATION OF ABSTRACT	18. NUMBER OF PAGES	19a. NAME OF RESPONSIBLE PERSON
a. REPORT	b. ABSTRACT	c. THIS PAGE			USAMRMC
U	U	U	UU	28	19b. TELEPHONE NUMBER (include area code)

Table of Contents

COVER.....	1
SF 298.....	2
Introduction.....	4-5
BODY.....	5-20
Key Research Accomplishments.....	21
Reportable Outcomes.....	22
Conclusions.....	23
References.....	24-27
Appendices.....	28

Introduction

Most diagnostic errors in radiographs are in areas with sub-optimal x-ray beam penetration. The large variations in transmitted x-ray intensity create serious problems in several radiographic applications. In many x-ray imaging situations the detection system must accommodate a large dynamic range. In mammography, it is necessary to detect low contrast lesions within a very large signal dynamic range that far exceeds the latitude of the detection system. Even today's most advanced digital detectors with large dynamic ranges are inadequate for imaging thick or dense breasts. There have been various attempts to devise a practical method for x-ray beam equalization in order to reduce the dynamic range of radiographic signals in medical x-ray images. X-ray beam equalization optimizes exposure and dose distribution throughout the entire breast by attenuating unnecessary exposure to thinner breast regions while preserving sufficient exposure to thicker breast regions. This spatially equalized exposure throughout the breast improves scatter-to-primary ratio, which increases contrast and optimizes contrast-to-noise ratio (CNR) throughout the image. The spatially equalized incident x-ray beam with a relatively narrow dynamic range could also greatly reduce the dynamic range requirements of the detection system. X-ray equalization also protect the detector from overexposure, which can cause irreversible decrease in sensitivity in most digital detectors and damage to electronic components (insulators, thin film capacitors, etc.) that have a limited tolerance to integrated radiation dose [1].

X-ray beam intensity modulation was initially introduced 70 years ago [2], and the concept was further evaluated in 1971 [3]. Since then, numerous attempts have been made to develop a clinically applicable device for x-ray beam equalization [4-10]. The x-ray beam equalization techniques can be divided into two groups: scanning equalization and area beam equalization.

In scanning equalization mammography systems [4, 5, 9, 10], a scanning pencil or fan beam is intensity modulated in accordance with density distribution of the patient. Scanning equalization systems improve image quality, but have significant disadvantages such as long scan times and substantial tube loading.

In area beam equalization, physical filters are positioned between the x-ray source and detector in order to equalize the photon flux to the detector. The thickness of the filter is adjusted in accordance with thickness or density distribution of the patient. A previous report has proposed to use pre-fabricated filters for different breast shapes [7]. This technique is potentially limited by image artifacts arising from filter-breast misalignment and the time required for positioning the most appropriate filter in the x-ray beam. Another study has proposed compressing an elastic reservoir, which contains a tissue-equivalent material, along with the breast [6]. It can provide patient specific equalization filter. However, it comes with the cost of increased scatter because of the contiguousness of the reservoir and breast. In addition, the tissue equivalent material may not be the best material to maintain contrast in the thinner regions of the breast.

Area beam equalization provides the benefits of short x-ray imaging time and reduced tube loading. A well known issue in area beam equalization is the beam hardening effect associated with physical attenuating filter that may reduce object contrast. However, optimal k-edge materials can actually enhance contrast and improve dose efficiency. These materials can be used as the filter material in x-ray beam equalization to provide both spectral shaping and intensity modulation. For example, in the case of a molybdenum (Mo) anode x-ray tube, a molybdenum filter is chosen in order to improve image quality and reduce patient dose. Calicchia *et al.* concluded that image contrast improved slightly with increasing molybdenum filtration up to 45-60 μm [32]. They also found that increasing the molybdenum filtration up to 75 μm significantly reduced entrance exposure and dose without loss of image quality for a film-screen system. Fahrig *et al.* reported that signal to noise ratio (SNR) per unit dose increases with the thickness of k-edge filter up to 0.14 g/cm² for digital mammography [11]. Although these studies have suggested the use of thicker filters (> 30 μm), thick uniform filters have not been implemented into clinical systems due to the fact that imaging thick breasts would result in excessive tube loading.

An optimally designed area beam equalization system, however, can implement the desired beam filtration to provide the benefits of patient dose reduction and image quality enhancement, such as increasing contrast and CNR, within tube loading limitations. Unlike uniform filtration that demands excessive tube loading, the mask in area beam equalization provides a spatially variable filter that accommodates for all

distributions of breast thicknesses and tube loading confines. For example, different thicknesses of filter are placed according to the regions corresponding to different thicknesses of the breast anatomy, where thicker filters are placed over thinner breast areas (such as the regions around the nipple) and thinner filters are placed over thicker breast areas (such as near the chest wall). Thus area beam equalization is a clinically beneficial technique for implementing optimal spectral modulation and dose distribution in mammography where previous uniform filter system could only provide conservative spectral shaping.

The above discussions indicate that a technique capable of area beam equalization would be a valuable tool in significantly improving the diagnostic quality of x-ray radiographs. However, the main limitation has been the technical difficulties involved with generating custom-made templates within the required time interval. The proposed x-ray beam equalization technique addresses this limitation. An array of 16x16 individually controlled square pistons will be used to generate a template [12-14]. A pre-exposure image will be used as a guide to position the individual pistons. The array of pistons will then be pressed against an attenuating mold of uniform thickness to generate a depth pattern for the equalization template. The template will be indexed into the x-ray beam before the acquisition of the final equalized image. The design goal of the system is to keep the time between the initial pre-exposure image and the final exposure under 5 seconds.

The proposed x-ray beam equalization technique can potentially have broad applications in many x-ray projection modalities such as coronary angiography, chest radiography and mammography. However, to date, the technical difficulties in generation of patient specific templates have hampered the clinical implementation of an area beam equalization technique. The proposed x-ray beam equalization technique addresses these technical limitations. The proposed technique can provide intensity modulation and optimal spectral shaping for different x-ray beam geometries such as area beam, scanning slot, and scanning multi-slit systems. Simulation and experimental studies will be conducted to optimize k-edge filter material for different anode/filter systems. Moreover, the potential of area beam equalization to improve image quality, reduce dose, and maximize dose efficiency by providing both intensity modulation and spectral shaping will be investigated quantitatively. The fundamentally improved equalized images can serve as the foundation from which better diagnosis and quantitative analysis can proceed.

1. Body of the report

Studies have been performed in the following areas:

- Estimation of detector dynamic range requirement for mammography.
- Prototype area beam equalization system.
- Multi-parameter optimization for area beam equalization mammography.
- Phantom studies of area beam equalization for a Mo/Mo x-ray source.
- Average glandular dose estimation with area beam equalization.
- Investigation of a new equalization prototype for clinical implementation.

1.1. Estimation of detector dynamic range requirement for mammography

X-ray equalization was first introduced for the film screen system because of its small dynamic range. Digital detectors have significantly improved dynamic ranges. The lack of experimental data leaves the question of whether their dynamic range is sufficient for mammography. Andrew *et al.* has estimated the dynamic range requirement for imaging a 5 cm breast to be approximately 3000 to 4000[15]. However, this approximation is based on a CCD coupled system with a relatively thinner phosphor screen. Moreover, Andrew *et al.* did not report the dynamic range requirement for imaging thick (>5 cm) breasts. A similar dynamic range estimation for both 5 and 8 cm breast is performed based on a CsI-aSi flat panel detector in the following analysis.

1.1.a. Theory

An ideal detector should be quantum limited even at the thick regions of the breast. For example, the electronic noise (σ_e) should be a fraction of x-ray quantum noise (σ_Q):

$$\sigma_Q = 3\sigma_e \quad (1)$$

Signal dynamic range is defined as [15]

$$\Gamma_s = \frac{Q_{open}}{k\sigma_Q}, \quad (2)$$

where Q_{open} is the signal at the open field, σ_Q is the quantum noise under the breast, $k = 5$ according to the Rose detectability model. Γ_s is the number of discernable gray levels in an image, and it indicates the maximum signal dynamic range limited by the quantum noise. The electronic dynamic range of a detector is defined as:

$$\Gamma_e = \frac{Q_{max}}{\sigma_e}. \quad (3)$$

Here Q_{max} is the maximum signal level limited by the detector. For an acceptable image, $Q_{open} < Q_{max}$. By combining Equations (1) to (3), the detector dynamic range requirement is derived:

$$\Gamma_e > 15 \cdot \Gamma_s \quad (4)$$

1.1.b. Simulation setup

A computer simulation program was written based on a previously reported technique to generate a mammography spectrum with a 0.5 keV resolution [16] for different target-filter combinations. A library of energy dependent mass attenuation coefficients based on published data was used to calculate the resultant transmission through various materials with a 0.5 keV resolution. Simulation parameters are shown in Table 1.

Table 1: Simulation parameters for dynamic range estimation

Detector	Inherent filter	Added filter			Compression paddle	Breast (BR12)	Contrast object
		Mo target	Rh target	W target			
200 μ m CsI 0.1x0.1 mm ² pixel	1 mm Be	30 μ m Mo	25 μ m Rh	1 mm Al	2.5 mm Lucite	5, 8 cm	0.1 mm μ -Ca

The pixel size is 0.1x0.1 mm². The total deposited energy inside one detector pixel is used as the signal (Q). Only the quantum statistical noise is considered in the simulation. Scatter is modulated based on scatter-primary-ratio (SPR):

$$\begin{aligned} Q &= Q_p(1 + SPR) \\ \sigma &= \sigma_p \sqrt{1 + SPR} \end{aligned} \quad (5)$$

With no anti-scatter grid, SPR was set to 0.7 and 1.2 for 5 cm and 8 cm breast thicknesses, respectively. Signal dynamic range Γ_s can be calculated using Equation (2). However, Γ_s depends on patient dose. Based on the Rose model, the level of dose is chosen to give a CNR of 5 for a 0.1 mm micro-calcification. Average glandular dose (AGD) is estimated using:

$$AGD = X \cdot D_{gN} \quad (6)$$

where X is the exposure to the breast and D_{gN} is the normalized average glandular dose [17-19].

1.1.c. Results

Table 2: Dynamic range estimation for different anode/filter and different breast thickness

Anode/filter	kVp	5cm Breast				8cm Breast			
		AGD (mGy)	Exp. (mR)	Γ_s	Required Γ_e	AGD (mGy)	Exp. (mR)	Γ_s	Required Γ_e
Mo/Mo	25	0.31	225	309	4640	2.55	3036	2820	42294
	26	0.29	204	283	4249	2.53	2895	2526	37890
	30	0.34	207	241	3619	2.72	2723	1709	25629
	35	0.43	238	208	3125	3.25	2876	1184	17763
Rh/Rh	25	0.29	186	227	3404	1.90	1971	1641	24621
	28	0.27	152	185	2770	1.60	1426	1167	17502
	30	0.28	143	170	2547	1.65	1334	1016	15235
	35	0.32	144	150	2245	1.80	1259	758	11376
W/Al	25	0.28	114	157	2349	1.53	955	911	13668

27	0.274	104	132	1980	1.33	762	660	9906
30	0.29	99	114	1711	1.20	615	483	7247
35	0.35	104	101	1511	1.31	570	361	5416
40	0.46	123	99	1478	1.75	675	327	4899

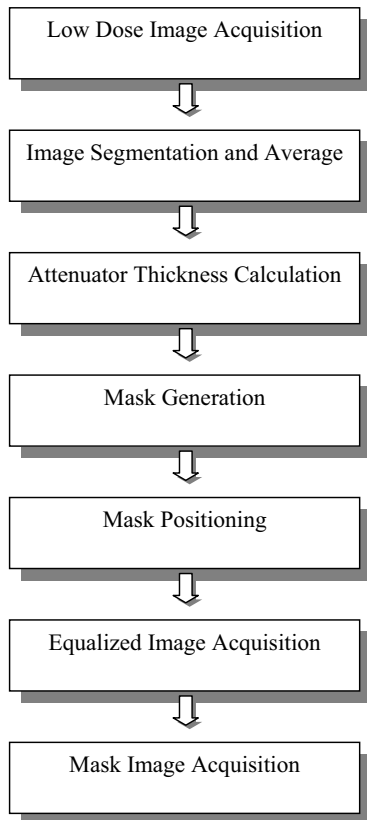
Table 2 shows the dynamic range estimation for different anode/filter systems and different breast thicknesses. For average sized breasts (5 cm), the current digital detectors almost meet the dynamic range requirements, even for Mo/Mo x-ray systems. However, larger breasts (8 cm) require much higher dynamic ranges. If the kVp is chosen based on minimal AGD (shaded lines), the required dynamic range exceeds that provided by most of the digital detectors. A limited detector dynamic range requires the use of higher kVp in order to maintain noise under the thick or dense breast regions within quantum limitation. However, using non-optimal kVp will result in higher AGD.

1.1.d. Conclusions

The above dynamic range analysis shows that x-ray beam equalization is necessary for imaging thick or dense breasts with a conventional mammography system. This is especially true in the case of systems using Mo or Rh anodes.

1.2. PROTOTYPE AREA BEAM EQUALIZATION SYSTEM

In area beam equalization, a patient-specific attenuation filter spatially modulates the x-ray beam intensity before it reaches the breast so that x-ray flux after the breast is approximately equalized. Areas corresponding to the low attenuating regions in the open field and around the nipple have thicker filters than areas corresponding to high attenuating regions near the chest wall. A detailed explanation of our prototype area beam equalization system, originally applied to coronary angiography, has previously been reported [13]. The original area beam equalization system has been upgraded from an 8 x 8 to a 16 x 16 array of individually controlled pistons to increase the filter resolution for mimicking compressed breast curvatures and local densities. A flow chart and a diagram of the combined digital mammography and area beam equalization system are shown in Figures 1 and 2.



Low-dose image acquisition

An initial low dose image is acquired with the digital detector and converted to an 8 bit, 2 x 2 binned image. The resulting digital image is then used for attenuator thickness calculations.

ATTENUATOR THICKNESS CALCULATION

Figure 1: Flow chart for an area x-ray beam equalization system for digital mammography.

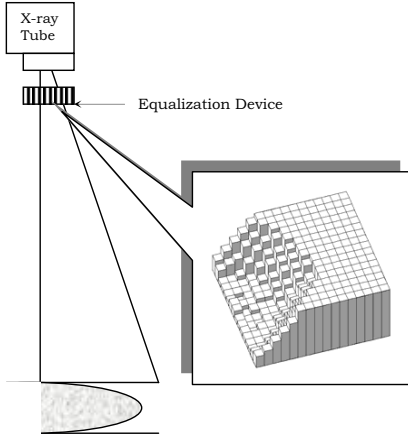


Figure 2: A diagram of area x-ray beam equalization applied to mammography. The equalization filter was fabricated by the equalization device and manually positioned in the x-ray beam at 12 cm from the focal spot.

EQ):

$$I_{target} = \frac{I_{max}}{EQ} \quad (7)$$

$$Ratio = \frac{I_{region}}{I_{target}} \quad (8)$$

$$\tau_A = 0 \quad \text{if } Ratio \leq 1 \quad (9)$$

$$\tau_A = [\alpha \ln(Ratio) + \beta] \ln(Ratio) \quad \text{if } Ratio > 1 \quad (10)$$

Equation 10 is used to calculate the mask thickness, where the coefficient α accounts for the spectral modulation effects caused by the mask. Attenuation ratios (Ratio) for different attenuator thicknesses were known from spectra modeling and were shown to agree well with experimentally determined attenuation ratios at approximately 0.2, 0.4, 0.6, and 0.8 cm of mask. The coefficients for Equation 10 are derived by a linear regression between the mask thicknesses versus the natural logarithm of the Ratio. The equalization mask is

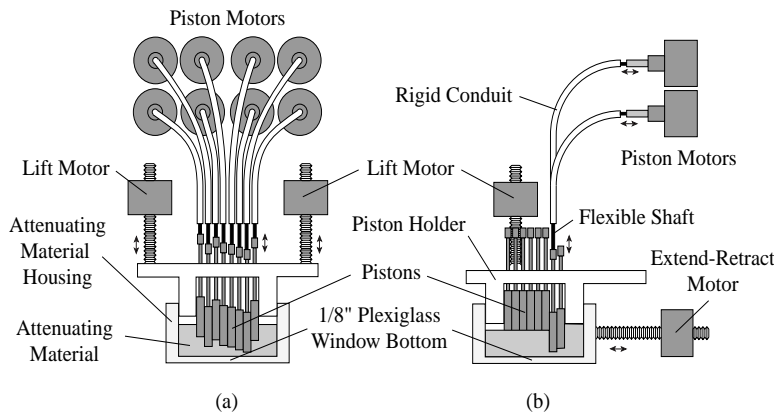


Figure 3. (a) Front view and (b) side view of the prototype device used to generate attenuating masks.

After acquisition of the initial unequalized image, it is segmented into a matrix of 16x16 square regions where the gray levels are transformed to derive a two-dimensional thickness profile of the equalization mask. Scatter correction with the convolution method is performed on the initial unequalized images to obtain a primary intensity only image [20]. The original image is convolved with a Gaussian-shaped scatter profile corresponding to a full-width at half-maximum (FWHM) of 2 cm [21, 22]. Scatter fraction as a function of gray level is determined from measuring the scatter fraction for different thicknesses of BR12 [20]. A scatter image is obtained from multiplying the blurred image with the scatter fraction lookup table. The scatter image is subtracted from the original image to obtain a primary only image. Then the attenuator thickness in cm (τ_A) for each matrix square is calculated from each region's average primary x-ray intensity (I_{region}), maximum average primary intensity in the image (I_{max}), and reduction magnitude of the primary intensity, henceforth known as Equalization Level (EQ):

generated from a deformable attenuation material made from a poly-dimethylsiloxane binder (Depco Inc., Hauppauge, NY) and molybdenum powder (Atlantic Equipment Engineers, Bergenfield, NJ) in an 8.6:1 binder to molybdenum powder weight/weight ratio. The equalization device provides a maximum mask thickness of 8.4 mm, which reduces the incident 28 kVp x-ray intensity by a factor of 55. For this attenuator, the coefficients α and β for calculating the attenuator thicknesses are 0.0105 cm and 0.165 cm, respectively.

Mask generation

A diagram of the prototype device for

equalization mask generation is shown in Figure 3. The equalization mask is fabricated using the deformable attenuation material described in the previous section. The attenuation material is confined within a 3.8 x 3.8 x 1.9 cm³ container. The attenuation material is initially flattened to a uniform thickness of 0.84 cm. An array of 16 x 16 square pistons, with dimensions of 0.159 x 0.159 cm², is then used to shape the attenuation material. The pistons are pushed into the material row by row using 16 stepper motors. For simplicity, only 8 motors were shown in Figure 3. An equalization mask with the desired two-dimensional thickness profile is generated by controllably pushing down on the attenuator to a target depth with the 256 pistons.

Mask positioning

After the mask is generated, it is separated from the pistons and manually positioned into a predefined location within the x-ray beam. The mask holder was placed immediately below the collimator of the mammography system to achieve the largest breast coverage on the flat panel detector. Future digital mammography equalization systems would have the mask positioned automatically.

1.3. Multi-parameter optimization for area beam equalization mammography

Multi-parameter optimization techniques for image quality and dose in mammography have been studied in depth [11, 23-31]. However, previous studies on image quality improvements from mammographic area beam equalization have been presented only qualitatively. There have been no previous reports on the optimization of attenuator material, tube voltage, and equalization level for area beam equalization in digital mammography. In this study, the optimal equalization parameters for digital mammography were determined using computer spectra simulation.

1.3.a. Method

A computer simulation program was written based on a previously reported technique to generate a molybdenum anode mammography spectrum with a 0.5 keV resolution [16]. A library of energy dependent mass attenuation coefficients based on published data was used to calculate the resultant transmission through various materials with a 0.5 keV resolution. Simulation studies were designed to mimic experimental conditions (elemental compositions and thicknesses of the inherent filter, equalization mask, phantoms, and detector components) closely. X-ray scatter was not included in the simulation. Simulation was validated by comparing the contrast (Figure 4) and HVLs (Table 3 on section 3.4.c) to those obtained by experiment.

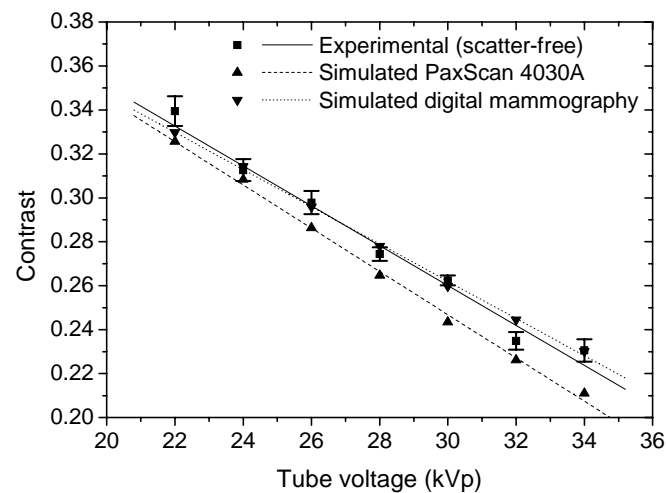


Figure 4: Experimental and simulated contrast as a function tube voltage for the Lucite contrast object on 50 mm BR12.

equalization. Changes in FOM, which is defined as the squared CNR divided by incident breast exposure, are also expressed as relative FOM:

$$FOM_{relative} = \frac{FOM}{FOM_o} = \frac{CNR^2/X}{CNR_o^2/X_o} \quad (11)$$

Computer simulations were initially conducted to determine optimal conditions for area beam equalization. First, contrast and relative CNR after equalization with attenuators composed of pure elements ranging from atomic numbers $Z=13$ (aluminum) to $Z=92$ (uranium) were calculated to select an attenuator that would give the best contrast and relative CNR with equalization. For each Z , an appropriate attenuator thickness was calculated iteratively with the bisection method to satisfy Equations 7-10. Second, the dependence of contrast, relative CNR, and relative FOM on kVp was investigated in order to select an optimal tube voltage for equalization of average size breasts. Third, contrast, relative CNR, and relative FOM for different equalization levels were calculated to determine an optimal equalization level based on image quality improvements versus increased exposure and tube loading considerations. Lastly, the previously mentioned three simulations were repeated for a clinical digital mammography detector in order to compare our results with a clinically relevant digital mammography system. The simulation code was changed to include acceptable properties of a clinical digital mammography detector. These properties included a $200\ \mu\text{m}$ CsI:Tl scintillating screen as well as a $0.25\ \text{mm}$ beryllium protective layer above the scintillator.

1.3.b. Results

Simulated contrasts for a level 20 equalization of $15\ \text{mm}$ of BR12 as a function of mask material, composed of a binder and pure attenuators ranging from $Z=13$ to $Z=92$ for 24, 26, 28, and 30 kVps, are shown in Figure 5a. Contrast generally decreases with kVp for all of the materials. However, an increase in contrast was observed at approximately $Z=42$ (Mo) for all kVps. Figure 5b shows simulated contrasts for an equalized $15\ \text{mm}$ BR12 using 28 kVp as a function of different atomic number mask materials for equalization levels of 5 to 40. As indicated by the arrow in Figure 5b, contrast remained fairly constant and even increased with increasing levels of equalization near $Z=42$. However, contrast can decrease up to 17% for $Z<35$ and $Z>48$ (e.g. from 0.306 to 0.254 for $Z=13$). Figure 6 shows the results for the optimization of relative FOM with kVp and equalization level for $15\ \text{mm}$ and $30\ \text{mm}$ of BR12. Relative FOM shows a maximum for equalized $15\ \text{mm}$ BR12 in the 28 kVp region. There were no observed local maxima in relative FOM within the 22 to 34 kVp range for $30\ \text{mm}$ and $50\ \text{mm}$ BR12. Figure 7 shows the improvement in relative FOM with equalization level for the $15\ \text{mm}$ region of the step phantom imaged at 28 kVp.

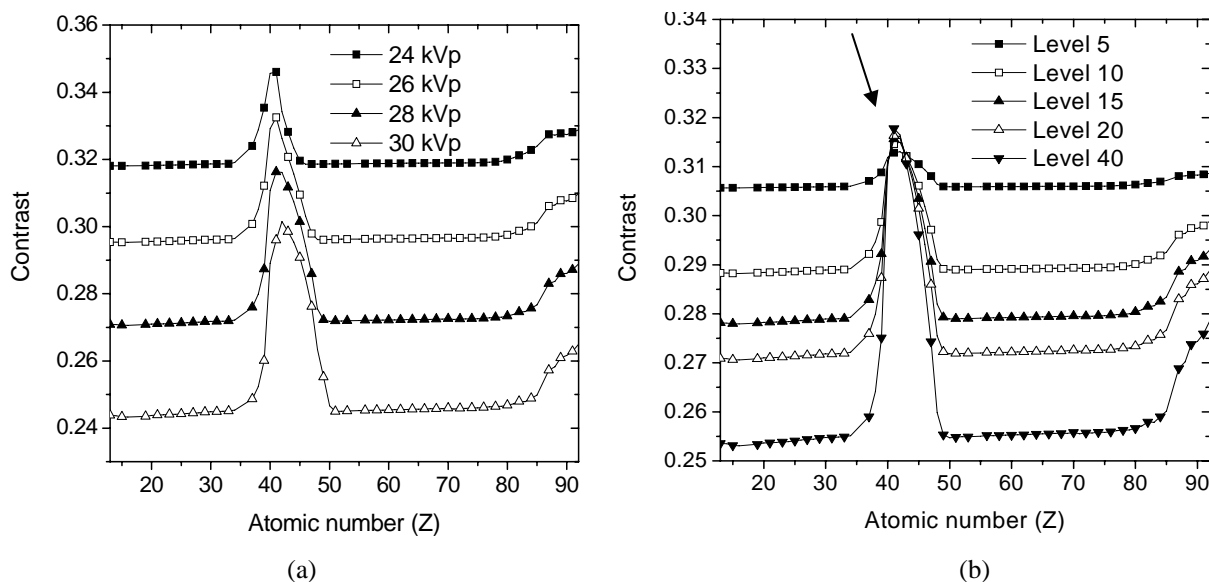


Figure 5: Simulated contrast versus attenuators made from different Z materials for the Lucite contrast object on $15\ \text{mm}$ BR12 for (a) different kVps (Level=20) and (b) different equalization levels (kVp=28). Entrance exposure to the $50\ \text{mm}$ region of the step phantom was kept constant at $100\ \text{mR}$.

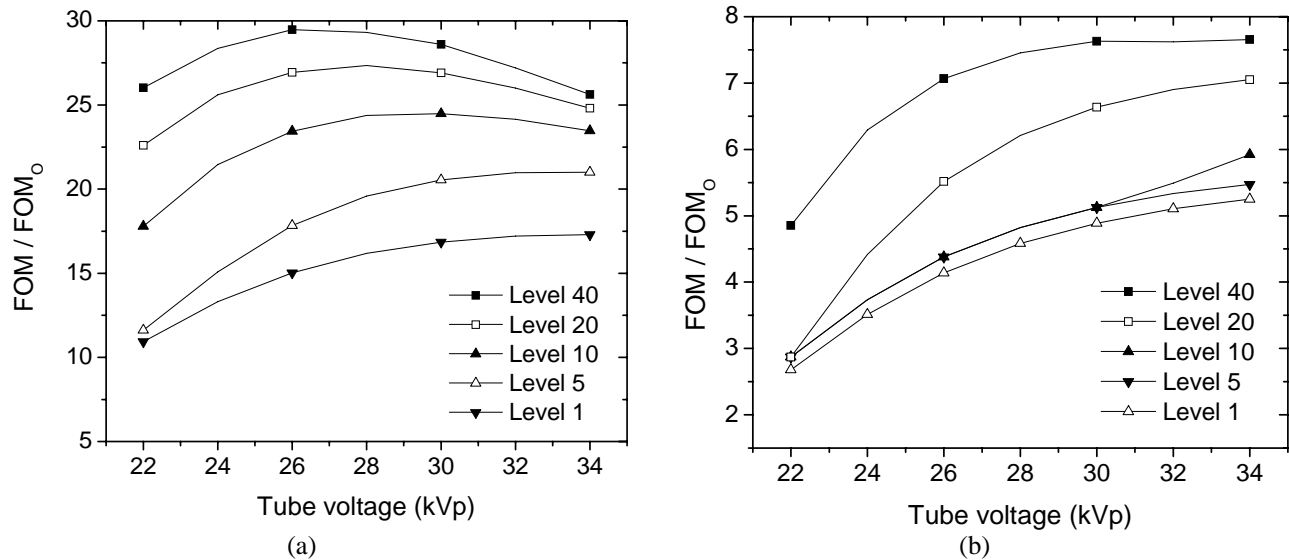


Figure 6: Simulated relative FOM as a function of tube voltage for the Lucite contrast object on (a) 15 mm BR12 and (b) 30 mm BR12 at various equalization levels. Entrance exposure to the 50 mm region of the step phantom was kept constant at 100 mR.

The response of contrast and relative FOM to different tube voltages at a constant exposure of 100 mR to the 50 mm BR12 region suggested that using a tube voltage in the range of 26 to 30 kV was optimal for imaging the step phantom with equalization. As expected, contrast on every step of the phantom decreased linearly with increasing kVp and relative noise decreased as attenuation decreased with tube voltage. The relative FOM for the 15 mm BR12 region reached a maximum by 26 kVp and 30 kVp for the higher and lower equalization levels, respectively. On the other hand, relative FOM increased less than linearly with kVp for both the 30 mm and 50 mm BR12 regions and approached a maximum in the region of 28 kVp for an equalization level of 40 (Figure 6).

1.3.c. Discussion

Attenuator material

In area beam equalization, the choice of attenuator material is very important. In addition to modulating the incident x-ray beam, it is essential to simultaneously optimize the x-ray beam spectra. Contrast was used as the primary parameter to optimize attenuator material. This is because both CNR and FOM can be improved with increasing kVp and equalization level. However, contrast would be degraded significantly for all kVp and equalization levels if an inappropriate material, such as aluminum or cerium, were to be used (Figures 5a and 5b). Most physical attenuators cause beam hardening, which degrades contrast. However, certain k-edge attenuator materials are capable of maintaining the same level of contrast or even improving it slightly. Simulation and experimental results show that a molybdenum based attenuator slightly improved contrast with increasing thickness up to 8 mm of mask material, which contained an equivalent of 10.2 μm of pure molybdenum.

Our results agree with previous reports on optimal filtration material for mammography [11, 32, 33]. In our study, contrast was observed to remain constant, even up to an equalization level of 48, or 8 mm of mask material. The total filtration including the inherent filter (21.5 μm molybdenum) and 8 mm of mask material (10.2 μm molybdenum) was 31.7 μm of molybdenum. Similarly, Calicchia *et al.* [32] concluded that image contrast improved slightly with increasing molybdenum filtration up to 45-60 μm . They also found that for a Mo/Mo system increasing the molybdenum filtration up to 75 μm significantly reduced entrance exposure and dose without loss of image quality for a film-screen system. Calicchia *et al.* [33] have also reported that a combined molybdenum and niobium filter improves contrast by approximately 8% for various thicknesses of Lucite phantoms. Fahrig and Yaffe [11] reported that a maximum signal-to-noise ratio (SNR) for a 200 μm calcification was achieved with filters made from niobium or molybdenum for a Mo/Mo system and a $\text{Gd}_2\text{O}_2\text{S}$ scintillating screen. Our results show that using molybdenum in the mask material allows area beam equalization to increase the fraction of photons in the 17-20 keV range by preferentially attenuating the lower

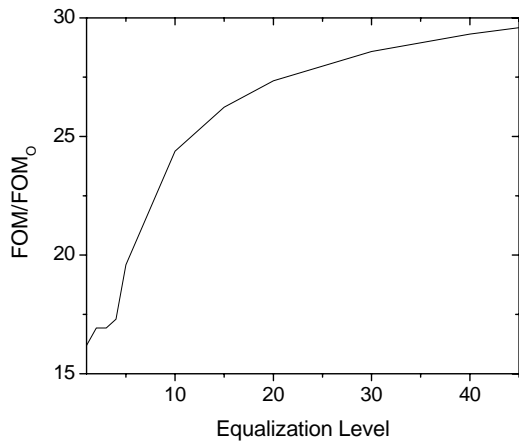


Figure 7: Simulated relative FOM versus equalization level for the Lucite contrast object on the 15 mm region of the step phantom using a tube voltage of 28 kVp. Entrance exposure to the 50 mm region of the step phantom was kept constant at 100 mR.

part will improve with increase of equalization level (Figure 7). The increase in FOM is due to the preferential attenuation of lower energy photons that have very low transmission through the breast, but would have contributed significantly to breast exposure. However, a high equalization level might result in a patient dose that is not practical or reduce the flux to the thin part too much so that SNR will drop below the detectability threshold. It is important to determine the optimal equalization level while minimizing both patient exposure and x-ray tube loading. This was done by calculating the FOM as a function of equalization level (see Figure 7). The results show that FOM increases with increasing equalization level and starts to plateau at approximately an equalization level of 20. This indicates that equalization levels higher than 20 are not justified. Furthermore, this level of equalization can reduce the signal dynamic range by a factor of 20, which will fit into the dynamic range of most digital detectors even for a very thick breast.

and higher energy photons. Figure 8 shows the change in incident spectrum with and without the equalization mask material. The beam spectrum after the equalization mask more closely resembles the beam exiting the BR12 phantom without equalization. Most of the photons below 15 keV are attenuated. Combined contrast enhancement with exposure reduction results from molybdenum filtration, which removes high energy (>20 keV) photons that degrade contrast and low energy (<17 keV) photons that primarily contribute to radiation risk without significant contribution to image formation.

Equalization level

In area beam equalization, no attenuator is placed in the region corresponding to the thickest part of the anatomy. By attenuating the regions corresponding to the thinner part of the anatomy, it is possible to increase the incident exposure to the thicker part of the anatomy. Therefore, CNR can be increased in the thicker part of the anatomy by the increased incident exposure to this region and reduced cross scatter from the thinner parts of the anatomy. Furthermore, FOM in the thin

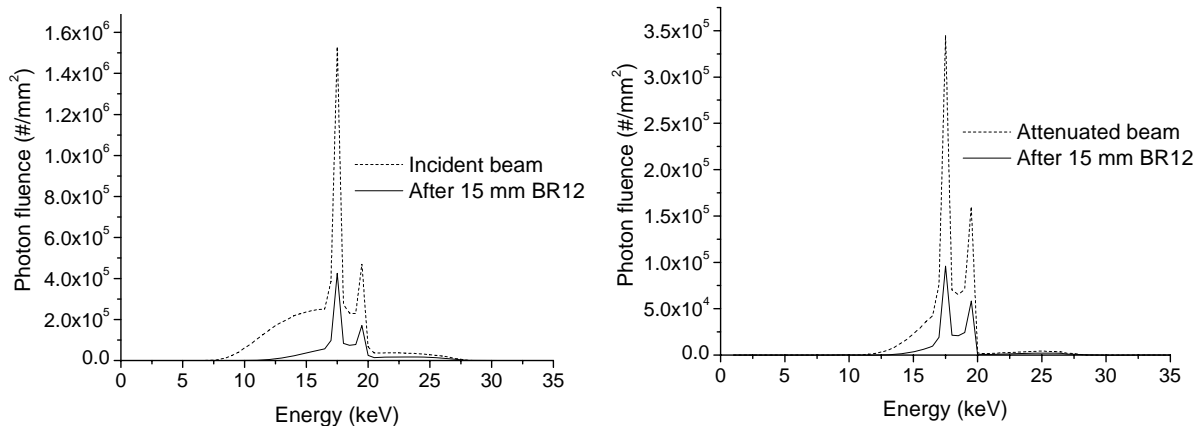


Figure 8: Spectral changes (a) without equalization filter and (b) with equalization filter.

1.3.d. Conclusions

The results of simulation studies showed that the ideal material to use for an attenuator in a Mo/Mo mammography system is molybdenum ($Z=42$). The use of a molybdenum based mask material in this study was shown to maintain image contrast with increasing attenuator thickness. FOM is improved with equalization because equalization provides variable thickness of k-edge filter (Mo), which produces optimal spectrum for different regions of the breast. An equalization level of 20 was chosen based on contrast, dose, and tube loading factors.

1.4. PHANTOM STUDIES OF AREA BEAM EQUALIZATION FOR A MO/MO X-RAY SOURCE

Analysis of simulation results revealed the optimal attenuation material, kVp, and equalization level for experimental studies on contrast, CNR, and FOM in equalization digital mammography. An attenuation material composed of 8.6:1 wt/wt ratio of poly-dimethylsiloxane binder and molybdenum powder (1 to 2 μm diameter) was made. A tube voltage of 28 kVp and an equalization level of 20 were chosen. Unless stated otherwise, images were acquired at 28 kVp and an equalization level of 20 was used for equalized images. Tube loading (mAs) for unequalized images was chosen to give maximal detector signal without saturation in the open field. With equalization, the mAs was increased to compensate for the mask attenuation.

1.4.a. Image acquisition

All images were acquired using a Profile-2000 mammography system (Trex Medical Corporation, Bennett Division, Copiague, NY), a PaxScan 4030A amorphous silicon digital x-ray detector (Varian Medical Systems, North Charleston, SC), and a focused Bucky grid (5:1 ratio, 31 lines/cm). The Profile-2000 mammography system consists of a M-2000G single-phase input high-frequency (100 kHz resonant) x-ray generator, molybdenum target, and 21.5 μm inherent molybdenum filter. The x-ray generator has a 22 to 35 kVp range. The PaxScan 4030A digital detector uses columnar CsI:Tl conversion screen technology. It has a 40 x 30 cm^2 effective detection window with a 194 μm pixel pitch, corresponding to a limiting resolution of 2.58 lp/mm. The source to image receptor distance (SID) was set at 75 cm.

1.4.b. Method

Scatter fraction, contrast, CNR, and FOM were determined for a step phantom under four conditions: (1) no grid and no equalization, (2) no grid but with equalization, (3) with grid but no equalization, and (4) with grid and with equalization. The step phantom used in this study was constructed from breast tissue equivalent material (BR12) and consisted of 15 mm, 30 mm, and 50 mm steps with edges 10 mm apart. In order to compare to simulation results, experimental contrast and CNR were adjusted for scatter according to the following equations:

$$\text{Contrast} = \frac{\text{Contrast}_{\text{exp}}}{(1 - SF)} \quad (12a)$$

$$\text{CNR} = \frac{\text{CNR}_{\text{exp}}}{\sqrt{1 - SF}} \quad (12b)$$

For images acquired without a grid, a 95% confidence interval for scatter fraction, contrast, CNR, and FOM were determined from error analysis of five identical measurements. Error analysis was not performed on images acquired with a bucky grid because subtle grid artifacts were visible at high digital magnification.

Half value layer

HVLs for 26, 28, and 30 kVp incident beams and HVLs for a 28 kVp beam attenuated with 3.4 mm, 5.0 mm, and 7.0 mm of the molybdenum based attenuation material were determined. A 6 cc mammography ion chamber (Model 20X6-6M-3, Radcal Corporation, Monrovia, CA) was used to measure the exposure from different beams filtered with increasing number of aluminum sheets. The recorded exposures were plotted with respect to the aluminum thickness and fitted to third-order polynomials. The HVLs were then interpolated from these polynomials.

Scatter Fraction

Scatter fractions were determined using lead discs with diameters 9.40 mm, 6.56 mm, 4.12 mm, and 2.50 mm. The scatter fraction at a zero lead disc diameter was then extrapolated from a linear regression analysis.

Contrast

The image contrast of the Lucite block (10 x 10 x 4.8 mm^3) was determined from images with and without the Lucite block. Average detected intensities within a defined 10 x 10 pixel square ROI covering a 100 pixel area at the center of the Lucite block (I_{Lucite}) and at the same location without the Lucite block ($I_{\text{background}}$) were determined. Contrasts for the Lucite block placed along the step edges at 15, 30, and 50 mm of BR12 were calculated.

Contrast-to-noise ratio

In calculating CNR for the Lucite block on the step phantom, relative noise was first determined. Two images of the step phantom were acquired under identical conditions. The images were then linearly subtracted to remove position-dependent non-uniformities that can affect the relative noise values. The standard deviation (σ) within a 10 x 10 square ROI of the subtracted image was determined and adjusted by $1/\sqrt{2}$ to account for the additive quantum noise from image subtraction. The corresponding CNR is computed from the contrast and relative noise ratio.

Figure of merit

FOM was calculated from the square of CNR divided by the entrance exposure in milli-Roentgen (mR) to the step phantom. Incident exposures with and without equalization were measured with a mammography ion chamber. In the cases for equalization, uniform thicknesses of the mask material (3.2 mm, 1.2 mm, and 0.0 mm) in the mask holder corresponding to the amount used in equalized images of the step phantom were placed in the beam. Then the entrance exposure to the step phantom was measured.

Breast Phantom Study

A compressed anthropomorphic breast phantom [34] was used to test the equalization with super-imposed micro-calcifications. Micro-calcifications in the range of 180-230 μm were isolated by filtering and collecting crushed calcium carbonate granules with 60 and 80 mesh sieves (Fisher Scientific, Hanover Park, IL). They were fixed onto a sheet of white paper using scotch tape. Nine micro-calcification particulates were arranged in a 3 x 3 array within a one cm^2 area with no overlap. An identical sheet of paper without micro-calcifications was placed in the x-ray beam during the gain calibration of the digital detector in order to remove the contrast from the scotch tape. The array of micro-calcifications was fixed onto the detector, and the breast phantom was placed on top of it. An unequalized image of the breast phantom with micro-calcifications was acquired using 28 kVp and 9.6 mAs without a grid. An equalized image was acquired using 28 kVp and 72 mAs without a grid. A mask image was acquired using 28 kVp and 9.6 mAs. To minimize noise, the mask image was smoothed by a 3 x 3 pixel running average kernel and subtracted from the equalized image. Both the unequalized and equalized images underwent identical intensity windowing to maximize micro-calcification contrast.

1.4.c. Results:

Diagnostic tests

The Profile-2000 mammography system showed a linear x-ray output in the experimental range of 8-280 mAs with an entrance exposure of 9.29 mR/mAs measured 75 cm from the focal spot. The PaxScan 4030A showed a linear response for detected intensities up to a pixel value of 8000 at a detector gain of 1, which corresponds to a detector entrance exposure of 52.2 mR. Beyond 8000, the detector showed saturation artifacts. Thus, the x-ray tube settings for unequalized and equalized images were chosen to be 9.6 mAs and 128 mAs, respectively. At these selected tube loadings, the gray levels in the region of the image with no phantom for unequalized and equalized images were approximately 7500 and 6000, respectively.

Half value layer

Table 3 organizes the experimental and simulation HVLs for different kVps and attenuator mask thicknesses. The simulation and experimental results are in good agreement.

Table 3: Experimental and simulated HVLs for different kVps and attenuator thicknesses.

Energy (kVp)	Attenuator thickness (mm)	HVL _{exp.} (mm Al)	HVL _{sim.} (mm Al)
26	0.0	0.26	0.26
28	0.0	0.28	0.28
30	0.0	0.29	0.30
28	3.4	0.48	0.49
28	5.0	0.51	0.52
28	7.0	0.55	0.54

Scatter Fraction, Contrast, CNR, FOM

Tables 4 and 5 show measured scatter fraction, contrast, CNR and FOM for different thicknesses of the step phantom with (Table 4) and without a grid (Table 5). Table 6 summarizes the scatter-free experimental and simulation contrasts at different BR12 thicknesses with and without equalization.

Table 4: Experimental scatter fraction, contrast, CNR, and FOM for the step phantom imaged without a grid. Unequalized and equalized images were acquired at 9.6 mAs and 128 mAs, respectively.

BR12 (mm)	UNEQUALIZED				EQUALIZED			
	SF	Contrast	CNR	FOM	SF	Contrast	CNR	FOM
15	0.174 +/-0.004	0.264 +/-0.003	68 +/-6	47 +/-9	0.206 +/-0.005	0.252 +/-0.001	109 +/-6	100 +/-12
30	0.274 +/-0.004	0.222 +/-0.002	34 +/-2	12 +/-2	0.252 +/-0.004	0.230 +/-0.001	100 +/-10	26 +/-5
50	0.448 +/-0.005	0.157 +/-0.001	12 +/-1	1.5 +/-0.4	0.333 +/-0.004	0.184 +/- 0.006	58 +/-4	2.8 +/-0.4

Table 5: Experimental scatter fraction, contrast, CNR, and FOM for the step phantom imaged with a grid. Unequalized and equalized images were acquired at 20 mAs and 280 mAs, respectively.

BR12 (mm)	UNEQUALIZED				EQUALIZED			
	SF	Contrast	CNR	FOM	SF	Contrast	CNR	FOM
15	0.152	0.261	59	17	0.146	0.296	127	62
30	0.205	0.242	35	6	0.148	0.267	107	13
50	0.276	0.215	16	1.2	0.193	0.217	83	2.6

Scatter fraction (SF) generally increased with increasing BR12 thickness. SF on the 15 mm BR12 region increased slightly when equalization was applied without grid. SF on the 50 mm BR12 region is significantly reduced when equalization applied either with or without grid. Contrast was improved with equalization. This was particularly apparent in the thickest part of the phantom where contrast increased from 15.7% when no equalization and grid were used to 21.7% when both equalization and grid were used. CNR increased with equalization for all thicknesses of the step phantom with and without a grid. The largest improvement with equalization was in the 50 mm BR12 region where CNR increased from 12 to 58 and 16 to 83 without and with grid, respectively. Equalization improved FOM for all thicknesses with or without a grid. Unlike CNR, the use of a grid and equalization did not have a synergistic effect on improving FOM. For all thicknesses of BR12, the lowest FOM was observed when only a grid was used and the highest FOM was observed when only equalization was utilized. This is consistent with the simulation that equalization filter will improve the FOM. The increase in FOM in the thickest region was mainly due to scatter reduction and subsequent contrast enhancement.

Table 6: Measured CNR and FOM of a step phantom with approximately the same CNR in the 15 mm region of the step phantom with and without equalization. Unequalized and equalized images were acquired at 9.6 mAs and 72 mAs, respectively. The CNR at 12mAs was estimated from that of 72mAs.

BR12 (mm)	Unequalized		Equalized		
	CNR (9.6mAs)	FOM	CNR (72mAs)	CNR (12mAs)	FOM
15	68	47	80	32	96
30	34	12	67	26	21
50	12	1.5	40	16	2.5

Breast Phantom Study

Figures 9 and 10 show breast phantom images with micro-calcifications without and with equalization. The unequalized and equalized images were acquired at 9.6 and 72 mAs, respectively. Square ROIs encompassing the 3 x 3 array of micro-calcifications are included in both images. Enlarged versions of the square ROIs with the micro-calcifications are also included. The window and level of both images have been adjusted to optimize micro-calcification visualization. The visualization of micro-calcification is improved in the equalized image as compared to the unequalized image.

1.4.d. Discussion

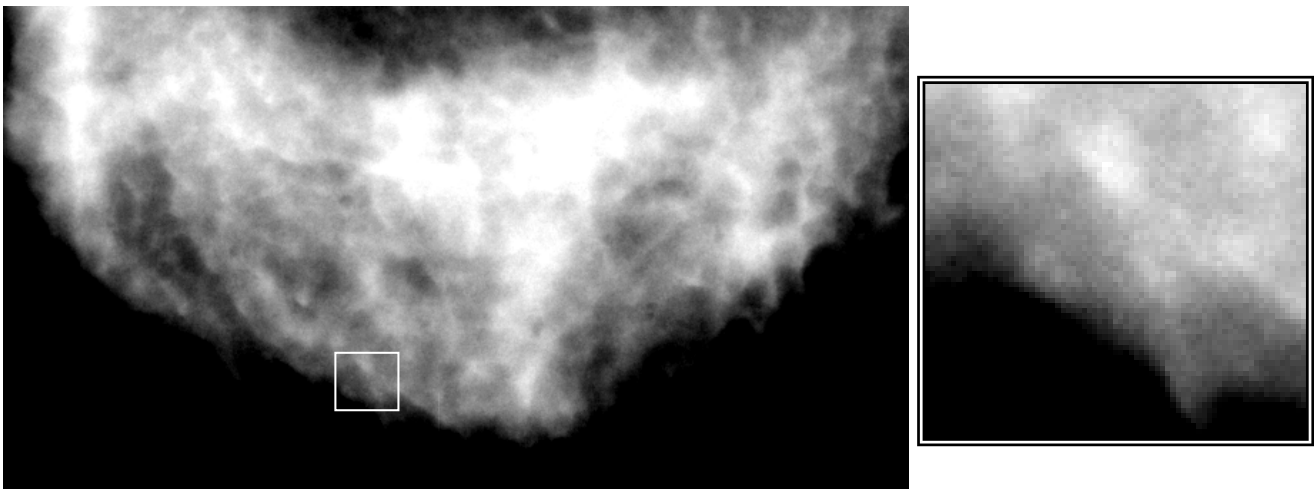


Figure 9: An unequalized image taken with 28 kVp and 9.6 mAs. The white squares encompasses the 3 x 3 array of 180-230 μm micro-calcifications, which are magnified on the right.

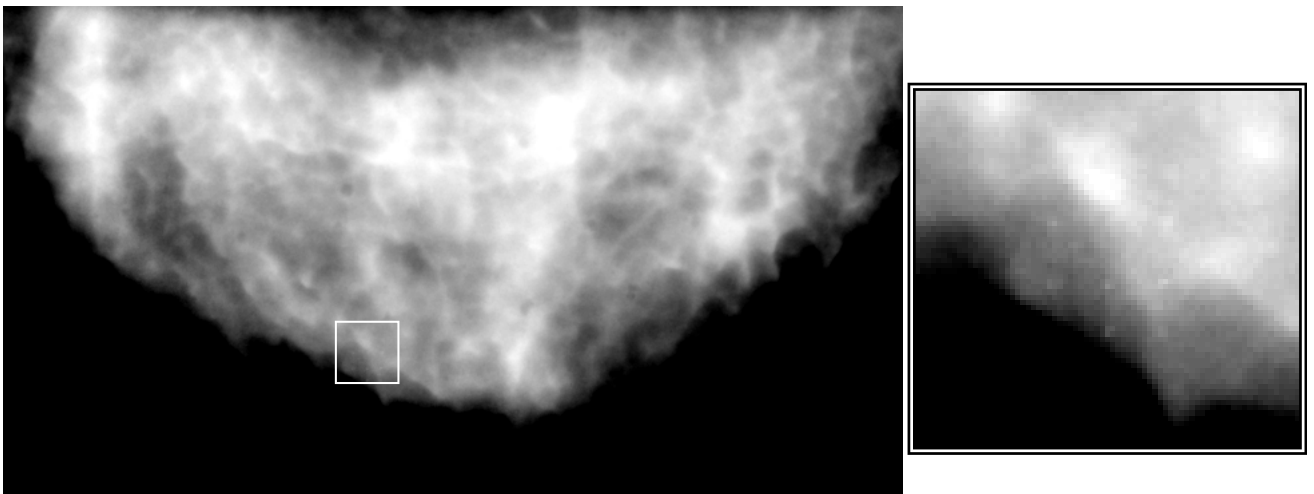


Figure 10: Image acquired with equalization with the mask subtracted and improved micro-calcification visualization. Image was taken with 28 kVp and 72 mAs. The white squares encompasses the 3 x 3 array of 180-230 μm micro-calcifications, which are magnified on the right.

Scatter fraction

Image contrast is reduced as the detected x-ray scatter is increased. Both an anti-scatter grid and air gap can be used to reduce scatter. An anti-scatter grid can successfully remove a large component of scatter throughout the image field, but the primary x-ray intensity is also attenuated by as much as 50%. Although air gaps have poorer scatter rejection capabilities than grids, air gaps of approximately 50 mm have been shown to have a better SNR improvement than grids for scatter fractions of 50% [35]. Equalization can also provide scatter fraction reduction to thick or dense breast regions by equalizing the primary intensity throughout the breast. However, equalization can also slightly increase the scatter fraction to the thinner breast regions because the primary intensities to these regions are reduced by equalization. This effect can be observed from the results for the 15 mm thickness of the step phantom shown in Table 4. The effect of scatter reduction for grid and equalization is cumulative. Equalization produces an image with approximately uniform scatter fraction and the grid reduces scatter in the entire image. Improvements in scatter fraction from using both equalization and grid are shown in Table 5.

Patient dose

An initial low dose image is required for area beam equalization. This can be accomplished with a minimal increase in the overall patient dose. It was possible to acquire the initial image using 1.3 mAs, which is the lowest possible setting for the mammography system. The image was adequate for calculating the 16x16 array of mask thicknesses. The average glandular dose under these conditions is only 0.02 mGy. It is anticipated that the patient dose can be further reduced by acquiring the initial image at lower mAs than that achievable with the current mammography system.

With equalization, it is possible to increase the x-ray flux in the thick part of the breast without saturating the detector in the periphery. For example, tube current was increased from 9.6 mAs to 128 mAs in the preliminary study as shown in Table 4. However, an exposure increase of this size can cause the patient dose to exceed the 3.0 mGy limit. Tube current was increased from 9.6 mAs to 72 mAs to keep the CNR at periphery to be the same as the conventional technique. However, the thinner peripheral region of a breast usually receives more x-ray flux than necessary. Therefore, it may be possible to reduce the x-ray flux in the thin region without compromising the detectability of lesions in this region. Taking the dose limitation in mind, there are 2 options:

Option 1. Maintain the same average glandular dose as conventional technique.

Option 2. Maximize the average glandular dose up to 3.0 mGy.

As will be shown in section 3.5, area beam equalization has been shown to decrease average glandular dose by 28% for a given incident exposure as compared to conventional mammography, which is due to the attenuation of incident photons to the thin parts of the breast. This portion of dose can be redistributed to the thick region by increasing the mAs by 28%. The tube current increased from 9.6 mAs to 12 mAs as shown in Table 6. Thus it is possible to perform equalization in mammography to obtain improved contrast and CNR in the thick portion of the breast without an increase in total dose. We anticipate that these two options can be implemented clinically as “low dose equalization method” (LEQ) and the “high dose equalization method” (HEQ), respectively.

Digital detector

Although the digital detector (PaxScan 4030A) used in the preliminary study was not designed for mammography applications, it provided good contrast and CNR for Lucite and micro-calcifications. The detector uses a thin protective layer of aluminum, which greatly reduces the transmittance of lower energy photons. A clinical digital mammography detector, such as the GE Revolution flat panel digital detector, would be expected to use a protective layer of beryllium instead of aluminum. This would reduce the attenuation of low energy photons and provide higher contrast and CNR for mammography. However, simulated results showed that the image contrast and CNR from our digital detector compared reasonably well with a clinical digital mammography detector (Figures 3 and 4). Therefore, the observed improvements in contrast and CNR with area beam equalization in this study should apply to studies performed with a clinical digital mammography system.

Another limitation of our digital detector for mammography applications is its spatial resolution of 194 μm as compared the GE digital detector, which has a pixel size of 100 μm [36]. However, with a contrast object of 1x1 cm^2 size, the effect of resolution on contrast and CNR measurement is negligible.

1.4.e. Conclusion

The physical phantom study confirmed simulation prediction that area beam equalization provides improved contrast and CNR to the thick/dense regions of breast without compromising the image quality in the thin regions. FOM for all regions was improved by approximately factor of two with equalization.

1.5. AVERAGE GLANDULAR DOSE ESTIMATION WITH AREA BEAM EQUALIZATION

The effect of equalization on glandular dose has not been previously studied. An estimated average glandular dose after equalization was calculated from the initial unequalized image of the breast and thickness of the corresponding equalization mask.

1.5.a. Method

Average glandular dose (\bar{D}_g) in milli-Gray (mGy) for a compressed anthropomorphic breast phantom [34] with and without equalization was computed from the product of the normalized average glandular dose (\bar{D}_{gN}) and entrance skin exposure (X_{ESE}):

$$\bar{D}_g = \bar{D}_{gN} \cdot X_{ESE} \quad (13)$$

In this study, \bar{D}_g , \bar{D}_{gN} , and X_{ESE} have units of mGy, mGy per Roentgen, and Roentgen, respectively. \bar{D}_g was determined semi-empirically from images of the breast phantom and the parameterized \bar{D}_{gN} . Following the method proposed by Sobol and Wu, $\bar{D}_{gN} = C\{V\{D\{H(HVL), d\}, kVp\}, c\}$ was calculated from the parameters of breast composition (c), tube voltage (kVp), breast thickness in cm (d), and HVL in mm aluminum [17]. The average glandular dose of the whole breast can be calculated from the sum of all pixelated $\bar{D}_{g,i}$ within an ROI in the mammogram weighted by the fraction of breast mass in the pixel (w_i) to the total breast mass (w_{total}):

$$\bar{D}_g = \sum_i \bar{D}_{g,i} \cdot \left(\frac{w_i}{w_{total}} \right) = \sum_i \bar{D}_{gN,i} \cdot X_{ESE,i} \cdot \left(\frac{w_i}{w_{total}} \right) \quad (14)$$

The breast composition, c, is constant at 50% glandular breast and the tube voltage is constant at 28 kVp. The breast thickness at each pixel (d_i) is derived from the mammogram. Assuming the effective linear attenuation coefficient of the breast phantom is not significantly affected by beam hardening, a breast thickness image can be derived from the unequalized mammogram. The HVL_i for the unequalized beam is constant at 0.28 mm aluminum. In the case of equalization, HVL_i increases as a function of attenuator thickness in cm (τ_A) according to the following best-fit polynomial to simulation data:

$$HVL_i = -2.0105\tau_A^4 + 4.3363\tau_A^3 - 3.4941\tau_A^2 + 1.3847\tau_A + 0.2807 \quad (15)$$

X_{ESE} is calculated from the initial exposure (X_{ESE}^o) and its attenuation due to an attenuator of thickness τ_A with an effective linear attenuation coefficient $\mu_{Attenuator}^{eff}$:

$$X_{ESE} = X_{ESE}^o \exp(-\mu_{Attenuator}^{eff} \cdot \tau_A) \quad (16)$$

$\mu_{Attenuator}^{eff}$ was determined to be 6.0 cm^{-1} . A software program was written that uses input images of the breast and mask and creates a weighted average glandular dose $\bar{D}_{g,i}$ image. An ROI around the breast region can be drawn manually. The total sum within this ROI gives the average glandular dose \bar{D}_g of the breast.

The above parameterization method assumes a uniform compressed breast for a limited range of breast thicknesses (3 to 8 cm) and HVLs (0.24 to 0.43). In an effort to calculate the average glandular dose, it was assumed that the \bar{D}_{gN} values near the nipple area are reasonably close to values of uniform breasts of the same thickness. In addition, \bar{D}_{gN} was extrapolated for breast thicknesses and HVLs outside the original tabulated ranges [18]. This extrapolation introduces acceptable errors because \bar{D}_{gN} depends linearly on HVL and bi-exponentially on breast thickness. Sobol and Wu have indicated that the errors associated with extrapolated \bar{D}_{gN} for breast thicknesses down to zero could be up to 15% [17].

1.5.b. Results

Table 7 shows the average glandular dose (AGD) for the breast phantom under various imaging conditions. The average glandular dose to the breast phantom (acquired using 28 kVp, 9.6 mAs, and no grid) was 0.16 mGy without equalization and 0.12 mGy with equalization. Thus, with the same entrance exposure, area beam equalization reduced the average glandular dose to the breast phantom by 25% (from 0.16 mGy to 0.12 mGy). This 25% dose reduction was due to the reduced entrance exposure to the thinner regions, increased beam hardening, and selective attenuation of low energy photons that do not contribute to the formation of the image.

Table 7: Average glandular dose approximations in mGy inside an area beam equalization ROI on a breast phantom for different imaging parameters.

	Unequalized		Equalized	
	mAs	mGy	mAs	mGy
Constant incident exposure	9.6	0.16	9.6	0.12

1.5.c. Conclusions

Area beam equalization can provide optimal dose distribution by reducing the dose to the periphery region, where the CNR is already very high, and redistribute the dose to the under penetrated thick/dense regions.

1.6. Investigation of a new equalization prototype for clinical implementation

Our current equalization prototype is adequate for phantom studies. However, it is not adequate for eventual clinical implementation. A smaller and faster device that can be easily maintained in a clinical environment is necessary. The current prototype equalization device can generate a filter within 30 seconds, which is too long for clinical applications. Therefore, a new equalization device is being designed. This device uses Ni(Ti) wire as an actuator rather than step motors. The Ni(Ti) wire can change length while being heated up to 70°C within 15 ms by an electrical pulse. The new method is proposed to generate a mask within 2 seconds.

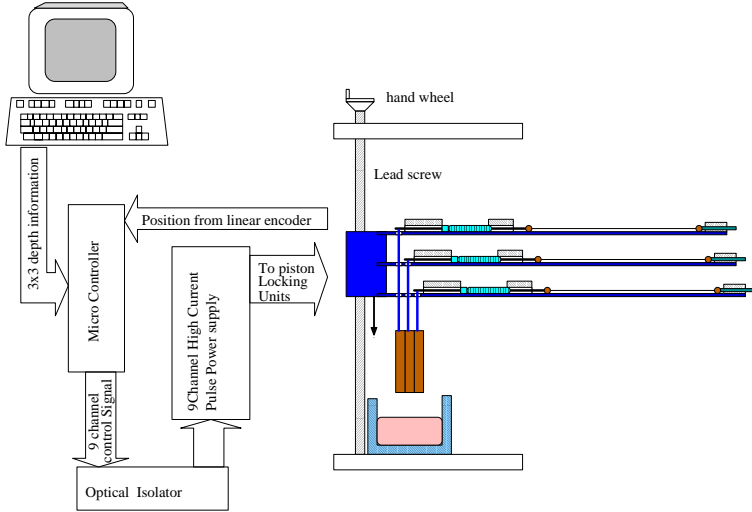


Figure 11 Block diagram of the 3x3 prototype

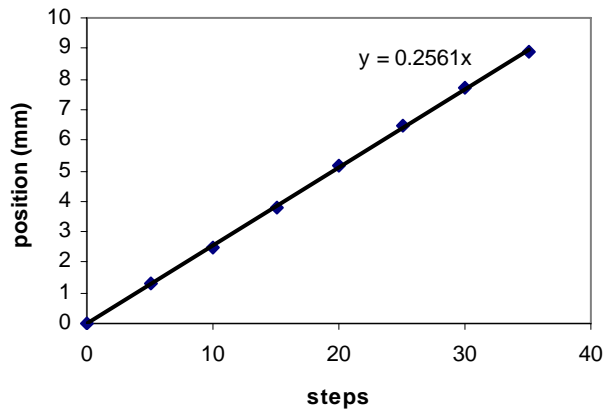


Figure 12 Measured depth of piston versus the preset depth in steps.

The principle of the new mask generation device is described in detail in section 4.3 and has been tested using a 3x3 prototype, which is shown in Figure 11. The piston module is driven by a hand wheel through a lead screw. A digital linear position encoder with a resolution of 4 counts/mm is used for the vertical position readout. Thus the mask can be generated with a step resolution of 0.25 mm/step. A control system based on a SX28AC (Uvicom Co.) micro-controller was built for our 3x3 prototype. The system is able to download the 3x3 depth information from the computer, acquire piston module position through a linear encoder, and position the 9 pistons at their desired respective positions. A high current pulse power supply is necessary to provide each Ni(Ti) wire with a 15 ms pulse of 7 A.

A 3x3 step filter was generated by this 3x3 prototype. The piston position ranged from 0 to 35 steps with 5 step intervals. The actual depth of each piston (relative to the 0 step) was measured using a caliper. The measured depth was plotted with respect to the preset step in Figure 12. A linear regression gives a slope of 0.256 mm/step, which is consistent with the step size of the linear encoder. The deviations between the measured depth and the fitted line give an RMS error of 0.074 mm. This is smaller than the truncation error introduced by the discrete step, which is half of the step size, 0.125 mm. This RMS error will introduce 7% error in the modulated x-ray intensity (using the linear attenuation coefficient of 6cm⁻¹

for 28 kVp Mo/Mo beam). It is anticipated that the depth error of the new device will have negligible change on the equalization level of the corresponding regions and it will not show any artifacts on the equalized image because the mask image will be subtracted from the equalized image.

2. Key Research Accomplishments

The key research accomplishments are the following:

1. Development of an area beam equalization system for mammography
2. Multi-parameter optimization for area beam equalization mammography
3. Phantom studies of area beam equalization for a Mo/Mo x-ray source
4. Average glandular dose estimation with area beam equalization

3. Reportable Outcomes

The results of x-ray beam equalization studies showed that the ideal material to use for an attenuator in a Mo/Mo mammography system is molybdenum ($Z = 42$). The use of a molybdenum-based mask material in this study was shown to maintain image contrast with increasing mask thickness. The details of the results have been reported and it is included in the appendix.

4. Conclusions

The results of x-ray beam equalization studies showed that the ideal material to use for an attenuator in a Mo/Mo mammography system is molybdenum ($Z = 42$). The use of a molybdenum-based mask material in this study was shown to maintain image contrast with increasing mask thickness. An equalization level of 20 was chosen based on contrast, average glandular dose and tube loading considerations. This study shows that area beam equalization can improve FOM in all regions of the breast. Area beam equalization in digital mammography can reduce patient dose while maintaining adequate CNR throughout the entire breast for lesion detection. It is expected that area beam equalization will improve the detection of nodules and micro-calcifications. Our phantom studies showed that visualization of microcalcification did improve after area beam equalization. However, the limited resolution of our digital detector limited our ability to extensively study the visualization of microcalcification after beam equalization.

5. References

1. Beutel, J., *Handbook of medical imaging*. 2000, Bellingham, Wash.: SPIE Press.
2. Hubbell, J.H. and S.M. Seltzer, *Tables of X-ray Mass Attenuation Coefficient and Mass Energy Absorption Coefficients 1 keV to 20 MeV for elements Z=1 to 92 and 48 Additional Substances of Dosimetric Interest*. 1995, NIST: Gaithersburg. p. 111.
3. Muller, S., *Full-field digital mammography designed as a complete system*. Eur J Radiol, 1999. **31**(1): p. 25-34.
4. Stefanoyiannis, A.P., et al., *A digital density equalization technique to improve visualization of breast periphery in mammography*. British Journal of Radiology, 2000. **73**(868): p. 410-20.
5. Pisano, E.D., et al., *Image processing algorithms for digital mammography: a pictorial essay*. Radiographics, 2000. **20**(5): p. 1479-91.
6. Edholm, P.R. and B. Jacobson, *Primary x-ray dodging*. Radiology, 1971. **99**(3): p. 694-6.
7. LaVoy, T.R., W. Huda, and K.F. Ogden, *Radiographic techniques in screen-film mammography*. Journal of Applied Clinical Medical Physics, 2002. **3**(3): p. 248-54.
8. Nishikawa, R.M., et al., *Scanned-projection digital mammography*. Medical Physics, 1987. **14**(5): p. 717-27.
9. Sabol, J.M., I.C. Soutar, and D.B. Plewes, *Mammographic scanning equalization radiography*. Medical Physics, 1993. **20**(5): p. 1505-15.
10. Sabol, J.M., I.C. Soutar, and D.B. Plewes, *Observer performance and dose efficiency of mammographic scanning equalization radiography*. Medical Physics, 1993. **20**(5): p. 1517-25.
11. Tesic, M.M., M.F. Piccaro, and B. Munier, *Full field digital mammography scanner*. Eur J Radiol, 1999. **31**(1): p. 2-17.
12. Kwok Leung, L. and C. Heang-Ping, *Effects of X-ray beam equalization on mammographic imaging*. Medical Physics, 1990. **17**(2): p. 242-9.
13. Goodsitt, M.M., et al., *Classification of compressed breast shapes for the design of equalization filters in x-ray mammography*. Medical Physics, 1998. **25**(6): p. 937-48.
14. Panayiotakis, G., et al., *Evaluation of an anatomical filter-based exposure equalization technique in mammography*. British Journal of Radiology, 1998. **71**(850): p. 1049-57.
15. Motz, J.W. and M. Danos, *Image information content and patient exposure (in radiography)*. Medical Physics, 1978. **5**(1): p. 8-22.
16. Jennings, R.J., et al., *Optimal X-ray spectra for screen-film mammography*. Medical Physics, 1981. **8**(5): p. 629-39.
17. Beaman, S.A. and S.C. Lillicrap, *Optimum X-ray spectra for mammography*. Physics in Medicine & Biology, 1982. **27**(10): p. 1209-20.
18. Muntz, E.P., et al., *An approach to specifying a minimum dose system for mammography using multiparameter optimization techniques*. Medical Physics, 1985. **12**(1): p. 5-12.
19. Fahrig, R. and M.J. Yaffe, *A model for optimization of spectral shape in digital mammography*. Medical Physics, 1994. **21**(9): p. 1463-71.
20. Fahrig, R. and M.J. Yaffe, *Optimization of spectral shape in digital mammography: dependence on anode material, breast thickness, and lesion type*. Medical Physics, 1994. **21**(9): p. 1473-81.
21. Court, L.E. and R. Speller, *A multiparameter optimization of digital mammography*. Physics in Medicine & Biology, 1995. **40**(11): p. 1841-61.
22. Huda, W., et al., *Experimental investigation of the dose and image quality characteristics of a digital mammography imaging system*. Medical Physics, 2003. **30**(3): p. 442-8.
23. Ogden, K.M., W. Huda, and E.M. Scalzetti. *A general approach to optimizing digital mammography with respect to radiation risk*. in *SPIE-Int. Soc. Opt. Eng. Proceedings of Spie - the International Society for Optical Engineering, vol.5030, 2003, pp.908-14*. USA. 2003.
24. Berns, E.A., R.E. Hendrick, and G.R. Cutter, *Optimization of technique factors for a silicon diode array full-field digital mammography system and comparison to screen-film mammography with matched average glandular dose*. Medical Physics, 2003. **30**(3): p. 334-40.

25. Molloi, S., et al., *Area X-ray beam equalization for digital angiography*. Medical Physics, 1999. **26**(12): p. 2684-92.
26. Molloi, S., A. Van Drie, and W. Fuming, *X-ray beam equalization: feasibility and performance of an automated prototype system in a phantom and swine*. Radiology, 2001. **221**(3): p. 668-75.
27. Xu, T., et al., *Area beam equalization: optimization and performance of an automated prototype system for chest radiography*. Academic Radiology, 2004. **11**(4): p. 377-389.
28. Molloi, S.Y. and C.A. Mistretta, *Scatter-glare corrections in quantitative dual-energy fluoroscopy*. Medical Physics, 1988. **15**(3): p. 289-97.
29. Boone, J.M., et al., *Scatter/primary in mammography: Comprehensive results*. Medical Physics, 2000. **27**(10): p. 2408-16.
30. Cooper, V.N., III, et al., *An edge spread technique for measurement of the scatter-to-primary ratio in mammography*. Medical Physics, 2000. **27**(5): p. 845-53.
31. Boone, J.M., T.R. Fewell, and R.J. Jennings, *Molybdenum, rhodium, and tungsten anode spectral models using interpolating polynomials with application to mammography*. Medical Physics, 1997. **24**(12): p. 1863-74.
32. Caldwell, C.B. and M.J. Yaffe, *Development of an anthropomorphic breast phantom*. Medical Physics, 1990. **17**(2): p. 273-80.
33. Sobol, W.T. and W. Xizeng, *Parametrization of mammography normalized average glandular dose tables*. Medical Physics, 1997. **24**(4): p. 547-54.
34. Wu, X., G.T. Barnes, and D.M. Tucker, *Spectral dependence of glandular tissue dose in screen-film mammography*. Radiology, 1991. **179**(1): p. 143-8.
35. Calicchia, A., et al., *Molybdenum filter optimization in mammography*. Physica Medica, 1994. **10**(2): p. 55-60.
36. Calicchia, A., et al., *Niobium/molybdenum K-edge filtration in mammography: contrast and dose evaluation*. Physics in Medicine & Biology, 1996. **41**(9): p. 1717-26.
37. Neitzel, U.,

1. Beutel, J., H.L. Kundel, and R.L. Van Metter, *Handbook of medical imaging*. 2000, Bellingham, Wash.: SPIE Press. v.
2. Fuchs, A.W., *Radiography of the entire body*. Med. Radiogr. Clin. Photogr., 1934. **10**: p. 9-14.
3. Edholm, P.R. and B. Jacobson, *Primary x-ray dodging*. Radiology, 1971. **99**(3): p. 694-6.
4. Sabol, J.M., I.C. Soutar, and D.B. Plewes, *Mammographic scanning equalization radiography*. Med Phys, 1993. **20**(5): p. 1505-15.
5. Sabol, J.M., I.C. Soutar, and D.B. Plewes, *Observer performance and dose efficiency of mammographic scanning equalization radiography*. Med Phys, 1993. **20**(5): p. 1517-25.
6. Kwok Leung, L. and C. Heang-Ping, *Effects of X-ray beam equalization on mammographic imaging*. Medical Physics, 1990. **17**(2): p. 242-9.
7. Goodsitt, M.M., et al., *Classification of compressed breast shapes for the design of equalization filters in x-ray mammography*. Med Phys, 1998. **25**(6): p. 937-48.
8. Panayiotakis, G., et al., *Evaluation of an anatomical filter-based exposure equalization technique in mammography*. Br J Radiol, 1998. **71**(850): p. 1049-57.
9. Sabol, J.M., I.C. Soutar, and D.B. Plewes, *Practical application of a scan-rotate equalization geometry to mammography*. Med Phys, 1996. **23**(12): p. 1987-96.
10. Sabol, J.M. and D.B. Plewes, *Analytical description of the high and low contrast behavior of a scan-rotate geometry for equalization mammography*. Med Phys, 1996. **23**(6): p. 887-98.
11. Fahrig, R. and M.J. Yaffe, *Optimization of spectral shape in digital mammography: dependence on anode material, breast thickness, and lesion type*. Med Phys, 1994. **21**(9): p. 1473-81.
12. Molloi, S., et al., *Area x-ray beam equalization for digital angiography*. Medical Physics, 1999. **26**(12): p. 2684-92.
13. Molloi, S., A. Van Drie, and F. Wang, *X-ray beam equalization: feasibility and performance of an automated prototype system in a phantom and swine*. Radiology, 2001. **221**(3): p. 668-75.

14. Xu, T., et al., *Area beam equalization: optimization and performance of an automated prototype system for chest radiography*. Acad Radiol, 2004. **11**(4): p. 377-89.
15. Maidment, A.D., R. Fahrig, and M.J. Yaffe, *Dynamic range requirements in digital mammography*. Med Phys, 1993. **20**(6): p. 1621-33.
16. Boone, J.M., T.R. Fewell, and R.J. Jennings, *Molybdenum, rhodium, and tungsten anode spectral models using interpolating polynomials with application to mammography*. Med Phys, 1997. **24**(12): p. 1863-74.
17. Sobol, W.T. and X. Wu, *Parametrization of mammography normalized average glandular dose tables*. Med Phys, 1997. **24**(4): p. 547-54.
18. Wu, X., G.T. Barnes, and D.M. Tucker, *Spectral dependence of glandular tissue dose in screen-film mammography*. Radiology, 1991. **179**(1): p. 143-8.
19. Rosentein, M., L.W. Andersen, and G.G. Warner, *Handbook of glandular tissue dose in Mammography*. Vol. FDA 85-8239. 1985: U.S. Dept. of Health and Human Services.
20. Molloy, S.Y. and C.A. Mistretta, *Scatter-glare corrections in quantitative dual-energy fluoroscopy*. Med Phys, 1988. **15**(3): p. 289-97.
21. Boone, J.M., et al., *Scatter/primary in mammography: Comprehensive results*. Medical Physics, 2000. **27**(10): p. 2408-16.
22. Cooper, V.N., 3rd, et al., *An edge spread technique for measurement of the scatter-to-primary ratio in mammography*. Med Phys, 2000. **27**(5): p. 845-53.
23. Motz, J.W. and M. Danos, *Image information content and patient exposure*. Med Phys, 1978. **5**(1): p. 8-22.
24. Jennings, R.J., et al., *Optimal x-ray spectra for screen-film mammography*. Med Phys, 1981. **8**(5): p. 629-39.
25. Beaman, S.A. and S.C. Lillicrap, *Optimum x-ray spectra for mammography*. Phys Med Biol, 1982. **27**(10): p. 1209-20.
26. Muntz, E.P., et al., *An approach to specifying a minimum dose system for mammography using multiparameter optimization techniques*. Med Phys, 1985. **12**(1): p. 5-12.
27. Fahrig, R. and M.J. Yaffe, *A model for optimization of spectral shape in digital mammography*. Med Phys, 1994. **21**(9): p. 1463-71.
28. Court, L.E. and R. Speller, *A multiparameter optimization of digital mammography*. Phys Med Biol, 1995. **40**(11): p. 1841-61.
29. Huda, W., et al., *Experimental investigation of the dose and image quality characteristics of a digital mammography imaging system*. Med Phys, 2003. **30**(3): p. 442-8.
30. Ogden, K.M., W. Huda, and E.M. Scalzetti. *A general approach to optimizing digital mammography with respect to radiation risk*. in *SPIE-Int. Soc. Opt. Eng. Proceedings of Spie - the International Society for Optical Engineering, vol.5030, 2003, pp.908-14*. USA. 2003.
31. Berns, E.A., R.E. Hendrick, and G.R. Cutter, *Optimization of technique factors for a silicon diode array full-field digital mammography system and comparison to screen-film mammography with matched average glandular dose*. Med Phys, 2003. **30**(3): p. 334-40.
32. Calicchia, A., et al., *Molybdenum filter optimization in mammography*. Physica Medica, 1994. **10**(2): p. 55-60.
33. Calicchia, A., et al., *Niobium/molybdenum K-edge filtration in mammography: contrast and dose evaluation*. Phys Med Biol, 1996. **41**(9): p. 1717-26.
34. Caldwell, C.B. and M.J. Yaffe, *Development of an anthropomorphic breast phantom*. Med Phys, 1990. **17**(2): p. 273-80.
35. Neitzel, U., *Grids or air gaps for scatter reduction in digital radiography: a model calculation*. Medical Physics, 1992. **19**(2): p. 475-81.
36. Muller, S., *Full-field digital mammography designed as a complete system*. European Journal of Radiology, 1999. **31**(1): p. 25-34.
37. Dance, D.R., et al., *Influence of anode/filter material and tube potential on contrast, signal-to-noise ratio and average absorbed dose in mammography: a Monte Carlo study*. Br J Radiol, 2000. **73**(874): p. 1056-67.

38. Pawluczyk, O., et al., *A volumetric method for estimation of breast density on digitized screen-film mammograms*. Med Phys, 2003. **30**(3): p. 352-64.
39. Chakraborty, D.P., *Proposed solution to the FROC problem and an invitation to collaborate*. Proceedings of Spie - the International Society for Optical Engineering, 2003. **5034**: p. 204-12.

6. Appendix

Wong J, Xu T, Husain A, Le H, Molloy S, “Effect of area x-ray beam equalization on image quality and dose in digital mammography” Physics in Medicine and Biology, 49:3539-3557, 2004.